Solid Friction Damping of Mechanical Vibrations

Philip R. Dahl*
The Aerospace Corporation, El Segundo, Calif.

A theory of solid friction damping of mechanical vibrations is presented that is based on a solid friction mathematical model previously proposed by the author. A summary and improved description of the general analytic features of the solid friction model are given as necessary background for the theory. The Coulomb friction damped oscillator is analyzed to establish an approach to the treatment of a simple friction damped oscillator. The approach then is generalized to treat a more general model of friction where the author's model is used to describe friction force primarily as a function of displacement. The solid friction damped oscillator studied is a wire pendulum where solid friction enters via inelastic flexing of the wire at the support. Theoretical results are generalized to be applicable to other types of oscillators and other sources of solid friction. An expression for the decay rate of the oscillation amplitude envelope of an unforced oscillator is derived. The decay rate and an equivalent linear damping ratio are determined for several values of an exponent parameter in the solid friction model.

I. Introduction

SOME simple tests were run on a wire sample to determine its natural damping characteristics. A weight was attached to the wire and the wire suspended as a simple pendulum under a vacuum. Amplitude of the oscillation was recorded upon release of the pendulum from an initial displacement. Analysis of the amplitude decay envelope data indicated a distinctively nonlinear damping behavior. It was apparent that a nonlinear model for damping was necessary to describe the pendulum damping over a wide range of deflection angles.

To describe the nonlinear behavior, it was thought that the author's model of solid friction, which was devised to describe bearing friction, likely would be applicable in describing the damping process, because the wire damping is the result of hysteretic work losses in the wire as it flexes back and forth in bending, and the solid friction model nicely simulates this type of process.

It was envisioned that it would be possible to investigate and analyze the nonlinear oscillation decay behavior in order to fit parameters of the friction model in the dynamics equation for the wire pendulum such that the observed behavior could be duplicated by simulation.

In the material that follows, a background and essential details of the author's solid friction model are presented. Next, the simple pendulum or spring/mass Coulomb friction damped oscillator is analyzed to show the general analytic approach employed. The general solid friction model then is introduced into the oscillator dynamics equation, and the relation of the damped oscillation amplitude to the solid friction energy dissipation per cycle is obtained. Further analysis yields the energy dissipation per cycle for several solid friction models. The oscillation amplitude decrement per cycle thereby is found as a function of amplitude, making it possible to integrate to obtain the oscillation decay envelope.

II. Background

In an Aerospace Corporation report,[1] a new math model of solid friction was formulated and presented by the author. The model slowly gained acceptance over the years and was used successfully by U.S. Government agencies and their contractors in simulation studies involving primarily ball bearing friction. Some of the studies known to the author have been published in the literature.[2-6] Improvements and extensions of the original model should be credited to Kuo and Singh,[2] Seltzer,[2,6] Nurre,[3] and Osborne and Rittenhouse.[5]

The mathematical model of solid friction that was formulated employs the observation that the time rate of change of solid friction can be expressed as

$$\frac{dF(x)}{dt} = \frac{dF(x)}{dx}\,\frac{dx}{dt} \tag{1}$$

where $F(x)$ is a solid friction force which is a function of displacement x only, and which has the characteristic shown in Fig. 1.

The friction force function $F(x)$ monotonically approaches $+F_C$ as long as $\dot{x}$ is positive. When the direction of motion is reversed, $\dot{x}<0$ and $F(x)$ follows the negative of its original shape and approaches $-F_C$. The friction function slope $dF(x)/dx$, however, remains positive at all times, even though $\dot{x}$ changes sign. It was discovered that this hysteretic behavior could be simulated with friction slope functions of the form

$$\frac{dF(x)}{dx} = \sigma\left|1-\frac{F}{F_c}\operatorname{sgn}\dot{x}\right|^{i}\operatorname{sgn}\left(1-\frac{F}{F_c}\operatorname{sgn}\dot{x}\right) \tag{2}$$

which are illustrated in Fig. 2 for positive velocities. The friction model is seen to behave as a nonlinear "soft" spring with a nearly linear elastic curve for small deflections, which yields and approaches a plastic curve for large deflections.

The quantity σ is the rest stiffness or slope of the force-deflection curve at $F=0$, and F_c is the Coulomb friction force which can also be thought of as a "yield force" or as "running friction force" (for example, as found in bearing friction).

Equations (1) and (2) can be used readily in simulations by employing the conceptual block diagram in Fig. 3. The operation of the friction model simulation loop in Fig. 3 is such that the Coulomb friction force $\pm F_c$ is approached asymptotically and, in principle, the slope function $dF(x)/dx$ need not be defined for $|F|>F_c$. However, in actual computer simulation practice, to ensure stability, the friction slope functions should have odd symmetry about the point $F/F_c=1$. This feature is provided by the multiplying factor, sgn $(1-(F/F_c)\operatorname{sgn}\dot{x})$. A small bias or feedback around the integrator in Fig. 3 also will take care of this stability problem.

Presented as Paper 75-1104 at the AIAA Guidance and Control Conference, Boston, Mass., Aug. 20-22, 1975; submitted Sept. 29, 1975; revision received Aug. 16, 1976.

Index categories: Computer Technology and Computer Simulation Technique; Spacecraft Attitude Dynamics and Control; Structural Dynamic Analysis.

*Staff Engineer, Electromechanical Dept., Guidance and Control Div. Member AIAA.

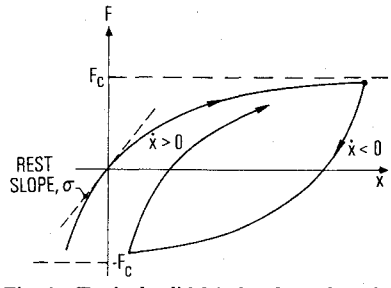

Fig. 1 Typical solid friction force function.

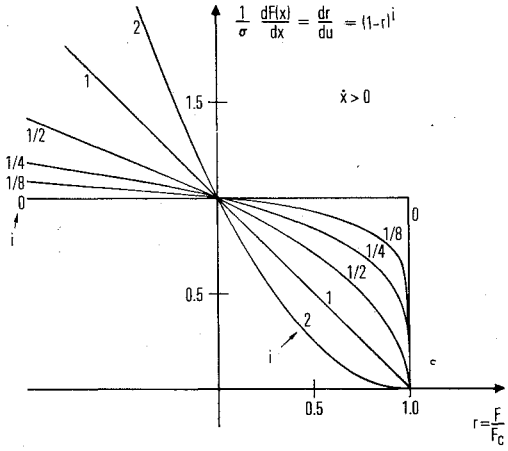

Fig. 2 Friction slope functions.

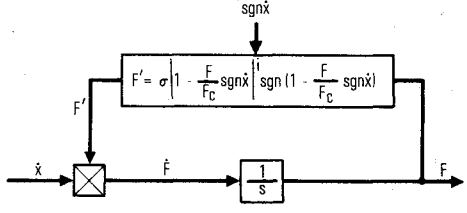

Fig. 3 Solid friction simulator.

The shape of the friction force-deflection functions $F(x)$ for positive velocities can be found by solution of Eq. (2) with $\text{sgn}\,\dot{x} = +1$. Introducing the dimensionless ratio

$$r = F/F_c \tag{3}$$

and using the initial condition $F(x) = 0$ at $x = 0$ give the result

$$r = 1 - [1 - (1-i)u]^{1/(1-i)} \tag{4}$$

with

$$u < \left(\frac{1}{1-i}\right) \text{ for } i < 1$$

where

$$u = \frac{x}{x_c} \tag{5}$$

is a dimensionless displacement variable, and x_c is a characteristic displacement defined by

$$x_c = \frac{F_c}{\sigma} \tag{6}$$

Several friction force-deflection functions given by Eq. (4) are shown in Fig. 4 for various values of the exponent i. The

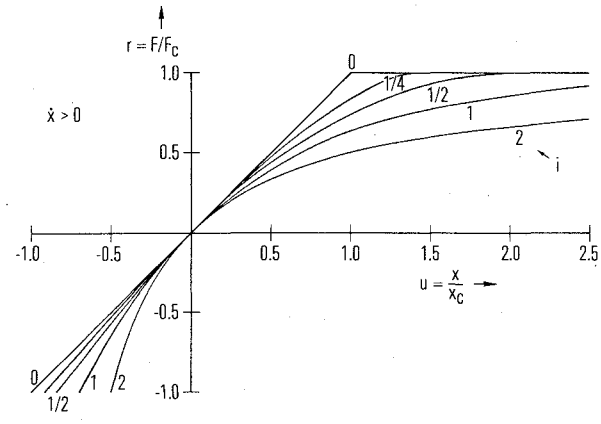

Fig. 4 Force/deflection functions.

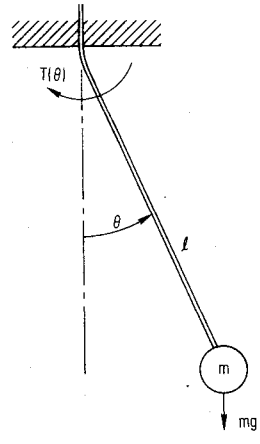

Fig. 5 Wire pendulum.

value of the parameter i defines the basic form of the friction functions and, hence, is used to describe the friction law being used. The functions given by Eqs. (2) and (4) give the same appearance as similar functions found and used by Iwan[7] to model hysteresis damping of structures. Equation (4) is also similar to an equation developed by Ramberg and Osgood[8] used to represent a wide range of stress-strain curves.

The force-deflection curves in Fig. 4 possess the characteristics of ductile type ($i = 1,2$), as well as brittle type ($i = 0$, ¼, ½) materials, and so a suitable solid friction model probably can be fit to the material being studied provided force-deflection test data can be obtained. It was found, however, that a single friction model is not adequate in some cases to simulate accurately the force-deflection data of some physical systems where minor hysteresis loops are considered. One solution to this problem is to employ additional friction models in parallel, with the output friction from each model being added to obtain the total friction. However, as Osborne and Rittenhouse[5] have pointed out, this approach may not be always sufficiently accurate to simulate nonsymmetric or off-axis minor hysteresis loops. Because the hysteresis loops considered in this paper are major loops that are essentially symmetric about the force-deflection origin, the accuracy of the single friction models has been found adequate.

III. The Solid Friction Damped Oscillator

Previous applications of the foregoing solid friction model have been used in studies of control systems where bearing friction was involved.[1-6] These studies showed that the model, when used in computer simulations of system dynamics, gave excellent agreement with test results. Seltzer[6] showed that the model can be used analytically to obtain describing functions for the nonlinear behavior of solid friction, thereby making it possible to predict the existence of and conditions for control system limit cycles due to nonlinear bearing friction. It is suggested that now it will be possible also to predict limit

cycles due to nonlinear structural damping because of the identical nature of the two phenomena.

The background theory of the solid friction model has been given, and it now will be applied to the general case of a simple, unforced, second-order oscillator containing solid friction damping. Results should be applicable to the damping of structural oscillations. First, however, the classic Coulomb friction damped oscillator will be discussed to establish an analytic baseline and to fix concepts.

A. Coulomb Friction Damped Oscillator

Consider a mass suspended as a pendulum by a wire as shown in Fig. 5. It is assumed that the wire remains straight, except for local bending at the support point. The equation of motion can be written

$$m\ell\,\ddot{\theta} = -mg\sin\theta - \frac{T(\theta)}{\ell} \tag{7}$$

where $T(\theta)$ is the opposing torque in the wire at the support, which is generally a nonlinear function of the pendulum deflection angle θ. Assuming θ small and using $\ddot{\theta} = \dot{\theta}(\mathrm{d}\dot{\theta}/\mathrm{d}\theta)$, Eq. (7) can be written as

$$\frac{m\ell^2}{2}\,\mathrm{d}(\dot{\theta}^2) + \frac{mg\ell}{2}\,\mathrm{d}(\theta^2) = -T(\theta)\,\mathrm{d}\theta \tag{8}$$

Let us examine the familiar case of Coulomb friction where, for the pendulum oscillator, the nonlinear torque function is defined by

$$T(\theta) = T_c \operatorname{sgn}\dot{\theta} \tag{9}$$

This form for $T(\theta)$ permits Eq. (8) to be integrated readily over a half cycle, where sgn $\dot{\theta}$ is constant. The result is

$$\dot{\theta}^2 + \frac{g}{\ell}\,\theta^2 = \frac{-2T_c \operatorname{sgn}\dot{\theta}}{m\ell^2}\,\theta + C_1 \tag{10}$$

where C_1 is a constant of integration. Recognizing that $\dot{\theta} = 0$ at the beginning of a half cycle allows Eq. (10) to be put in the form

$$\dot{\theta}^2 + (g/\ell)\,(\theta + \theta_c \operatorname{sgn}\dot{\theta})^2 = R^2 \tag{11}$$

where

$$R^2 = (g/\ell)\,(\theta_1 - \theta_c)^2 \tag{12}$$

θ_1 = magnitude of displacement at beginning of half cycle, and

$$\theta_c = T_c/mg\ell \tag{13}$$

The amplitude decay rate or the change in amplitude per cycle is

$$\mathrm{d}\bar{\theta}/\mathrm{d}N = -2\Delta\theta \tag{14}$$

where N is the cycle number, $\bar{\theta}$ is the amplitude at the beginning of the cycle, and $\Delta\theta$ is the decrease in amplitude in one-half cycle, which is deduced to be

$$\Delta\theta = 2\theta_c \tag{15}$$

It is noted that the energy dissipated per half cycle, ΔE, due to the Coulomb friction, is

$$\Delta E = 2T_c\bar{\theta} \tag{16}$$

We now introduce the spring rate k_n of an equivalent spring mass oscillator

$$k_n = mg\ell \tag{17}$$

and employ Eqs. (13), (15), and (16) in (14) to obtain

$$\frac{\mathrm{d}\bar{\theta}}{\mathrm{d}N} = \frac{-4T_c}{k_n} \tag{18}$$

or

$$\frac{\mathrm{d}\bar{\theta}}{\mathrm{d}N} = \frac{-2\Delta E}{k_n\bar{\theta}} \tag{19}$$

It will be seen that Eq. (16) is a limiting form of a more general relation for energy dissipated per half cycle, and that Eq. (19) is the relation for the amplitude decay rate of solid friction damped systems.

Equation (18) can be integrated directly to obtain the decay envelope relation

$$(\theta - \theta_0) = \frac{-4T_c}{kn}N \tag{20}$$

where θ_0 is the initial amplitude at $N = 0$. Equation (20) shows the linear nature of the oscillation decay envelope of classical Coulomb friction for $\theta > \theta_c$.

B. General Solid Friction Damped Oscillator

Let us proceed again from Eq. (7) and rephrase this solid friction damped oscillator equation by using the defining Eq. (17) for k_n. Equation (7) becomes, employing the approximation $\sin\theta \approx \theta$

$$m\ell^2\ddot{\theta} = -k_n\theta - T(\theta) \tag{21}$$

We use $\ddot{\theta} = \dot{\theta}\,\mathrm{d}\dot{\theta}/\mathrm{d}\theta$ in Eq. (21) and integrate to find

$$m\ell^2\int_{\dot{\theta}_1}^{\dot{\theta}_2}\dot{\theta}\,\mathrm{d}\dot{\theta} + \int_{\theta_1}^{\theta_2}[k_n\theta + T(\theta)]\,\mathrm{d}\theta = 0 \tag{22}$$

or

$$\frac{m\ell^2}{2}\,(\dot{\theta}_2^2 - \dot{\theta}_1^2) + \frac{k_n}{2}\,(\theta_2^2 - \theta_1^2) = -\int_{\theta_1}^{\theta_2}T(\theta)\,\mathrm{d}\theta \tag{23}$$

If we choose the limits of integration to be the extremes of a half cycle of motion, then $\dot{\theta}_2$ and $\dot{\theta}_1$ are zero and the first term in Eqs. (22) and (23) will be zero. Under these conditions, Eq. (22) becomes

$$\int_{\theta_1}^{\theta_2}[k_n\theta + T(\theta)]\,\mathrm{d}\theta = 0 \tag{24}$$

1. *Nonlinear "Spring" Only*

Let us now examine the nature of this integral for the case where the oscillator does not possess a linear spring, i.e., $k_n = 0$. We then have the nonlinear "spring" possessing damping characteristics,

$$\int_{\theta_1}^{\theta_2}T(\theta)\,\mathrm{d}\theta = 0 \tag{25}$$

or, in terms of the nondimensional variables r and u,

$$\int_{u_1}^{u_2}r(u)\,\mathrm{d}u = 0 \tag{26}$$

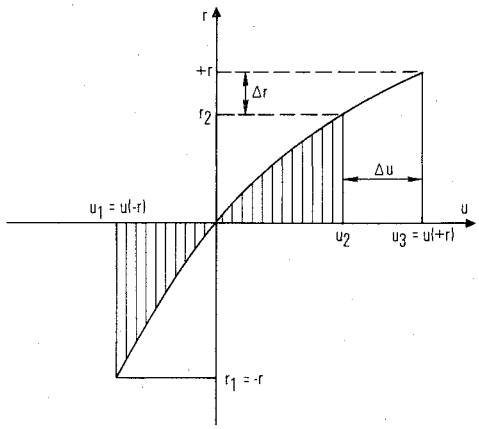

Fig. 6 Amplitude decrement in a half cycle.

This relation is illustrated in Fig. 6, which shows the integral between the limits u_1 and u_2 to be zero, i.e., the shaded areas are equal. The torque-deflection curve from $u_1 = u(-r)$ is shown extended past u_2 to the point $u_3 = u(+r)$. It is seen from the figure that

$$\int_{u_1}^{u_2} r\,du = \int_{u_1}^{u_3} r\,du - \int_{u_2}^{u_3} r\,du \tag{27}$$

and that

$$\int_{u_2}^{u_3} r\,du \approx \left(r - \frac{\Delta r}{2}\right)\Delta u \approx r\Delta u \tag{28}$$

where Δr is assumed to be small compared to r. Substituting Eqs. (26) and (28) into (27) then results in

$$r\Delta u = \int_{u_1}^{u_3} r\,du \tag{29}$$

The quantity Δu is the decrement in the amplitude of oscillation per half cycle. This interpretation of Δu is explained as follows.

Suppose that a small amount of energy were added each half cycle, such that the magnitudes of the maximum restoring torque at the extremes of a half cycle of motion were equal. Under this condition, the peak-to-peak amplitude of the oscillatory motion would be sustained and would neither increase nor decrease. Thus, it can be seen that an oscillation with no decay would swing over a range from u_1 to u_3. It follows, therefore, that Δu represents the loss in amplitude over a half cycle.

We now define the amplitude $\bar{u}$

$$\bar{u} = \frac{u(+r) - u(-r)}{2} \tag{30}$$

which is seen to be the amplitude of the damped oscillator at the beginning of the half cycle. The amplitude at the end of the half cycle is obviously

$$\bar{u}_{j+1} = \bar{u}_j - \Delta u \tag{31}$$

where j denotes the half cycle number.

It becomes apparent that the amount of energy that must be added to sustain the amplitude of oscillation is the area under the torque deflection curve from u_2 to u_3, and that this must be equal to ΔE, the energy dissipated over the half cycle due to solid friction. We therefore define ΔE generally as the quantity on the right-hand side of Eq. (29). After denormalizing,

$$\Delta E = T_c\theta_c \int_{u_1}^{u_3} r\,du \tag{32}$$

2. Linear and Nonlinear Springs in Parallel

It is now possible to apply this approach to the case where a linear spring is in parallel with the nonlinear spring such that Eq. (24) applies. In terms of the nondimensional variables, Eq. (24) becomes

$$\int_{u_1}^{u_2}\left(\frac{k_n}{\sigma}u + r\right)du = 0 \tag{33}$$

Referring to Fig. 7 for this case and following the same procedure as before, we have

$$0 = \int_{u_1}^{u_3}\frac{k_n}{\sigma}u\,du - \int_{u_2}^{u_3}\frac{k_n}{\sigma}u\,du + \int_{u_1}^{u_3} r\,du - \int_{u_2}^{u_3} r\,du \tag{34}$$

The first term in Eq. (34) is zero, the second term can be approximated by $(k_n/\sigma)\bar{u}\Delta u$, and the remaining terms have been found previously, which leads us to a relation similar in form to Eq. (29)

$$\left(r(\bar{u}) + \frac{k_n}{\sigma}\bar{u}\right)\Delta u = \int_{u_1}^{u_3} r\,du \tag{35}$$

Denormalizing Eq. (35) and using Eq. (32) gives

$$\Delta\theta = \frac{\Delta E}{T(\bar{\theta}) + k_n\bar{\theta}} \tag{36}$$

where

$$\bar{\theta} = \theta_c\bar{u} \tag{37}$$

Using Eq. (14) in (36) gives

$$\frac{d\bar{\theta}}{dN} = \frac{-2\Delta E}{T(\bar{\theta}) + k_n\bar{\theta}} \tag{38}$$

which corresponds to Eq. (19) for simple Coulomb friction if $T(\bar{\theta}) << k_n\bar{\theta}$. At large amplitudes, the nonlinear friction torque is saturated such that $T(\bar{\theta}) \approx T_c$ will usually be small compared to $k_n\bar{\theta}$. At low amplitudes, the wire is nearly elastic, and $T(\bar{\theta}) \approx \sigma\theta$ and Eq. (38) becomes

$$\frac{d\bar{\theta}}{dN} = -\frac{2\Delta E}{(\sigma + k_n)\bar{\theta}} \tag{39}$$

indicating as may be expected that at low amplitudes, the nonlinear friction element behaves as a spring where its rest stiffness σ adds in parallel with the linear stiffness k_n.

Equation (36) for the amplitude decay is viewed as being basic for solid friction damped oscillators and in conjunction with the difference equation given by Eq. (31) permits determination of the oscillation decay envelope. Alternatively, solution of the differential equation given by Eq. (38) also will give the oscillation decay envelope as a function of N. Equation (38) also can be used as a basis for comparison with the damping characteristics of a linear viscous damped oscillator which has an amplitude decay rate given by

$$\frac{d\bar{\theta}}{dN} = -2\pi\zeta\bar{\theta} \tag{40}$$

where ζ is an equivalent linear damping ratio. Then, comparing Eq. (38) with (40), we deduce that the equivalent linear damping ratio can be expressed as

$$\zeta = \frac{\Delta E}{\pi\bar{\theta}(k_n\bar{\theta} + T(\bar{\theta}))} \tag{41}$$

IV. Solid Friction Damping

The foregoing examination of the general case of damping of an oscillator via the mechanism of solid friction has indicated that the amplitude decay rate, the amplitude decay envelope, and an equivalent linear damping ratio can be determined if analytical expressions can be found for the solid friction energy dissipation. We shall proceed to do this using force-deflection functions expressed by Eq. (4).

A. Solid Friction Energy Dissipation

The energy loss due to hysteretic solid friction damping over a half cycle has been defined by Eq. (32). It also can be expressed as

$$\frac{\Delta E}{2T_c\theta_c} = \frac{1}{2}\int_{u(-r)}^{u(+r)} r\,du \tag{42}$$

Alternatively, the integration in Eq. (42) can be carried out with respect to torque rather than displacement using the expression

$$\Delta E = \int_{-T}^{T} \frac{T}{dT/d\theta}\,dT \tag{43}$$

or, in terms of the dimensionless variables r and u,

$$\frac{\Delta E(r)}{2T_c\theta_c} = \frac{1}{2}\int_{-r}^{r} \frac{r}{(dr/du)\,(A)}\,dr \tag{44}$$

After integration, ΔE can be found as a function of u, the displacement variable, by substitution of $r=r(u)$ from Eq. (4) into Eq. (44). However, the amplitude at the beginning of a half cycle is not the same as u, but is equal to $\bar{u}$ given by Eq. (30). We therefore evaluate $r=r(\bar{u})$ and substitute into the solution of Eq. (44) to find $\Delta E(\bar{u})/2T_c\theta_c$. The results for $i=0, 1, 2$ are

$$\frac{\Delta E}{2T_c\theta_c}(\bar{u}) = \begin{cases} \left(\begin{matrix} 0, \bar{u}<1 \\ (\bar{u}-1), \bar{u}>1 \end{matrix}\right), & i=0 \\ \bar{u}-\tanh\bar{u}, & i=1 \\ \bar{u}-\tfrac{1}{2}\ln\left[\dfrac{1+r(\bar{u})}{1-r(\bar{u})}\right], & i=2 \end{cases} \tag{45}$$

It is seen that the $\Delta E(\bar{u})/2T_c\theta_c$ functions for various values of i reveal that they have a general form involving two terms, the first of which is $\bar{u}$. The second term becomes small compared to $\bar{u}$ as $\bar{u}$ gets large. For $\bar{u}>>1$, it is found that $\Delta E(\bar{u})/2T_c\theta_c$ may be approximated by $\bar{u}$ or that

$$\Delta E(\bar{\theta}) \approx 2T_c\bar{\theta}, \quad \bar{\theta}>>\theta_c \tag{46}$$

which is identical to Eq. (16) found for the simple Coulomb models.

An important approximation for the energy dissipation at low amplitudes is found by assuming $r<<1$ in the $\Delta E(r)/2T_c\theta_c$ expression for general i values. Using the first terms in the binomial expansions up to the r^3 term for the $(1\pm r)$ quantities [in the $\Delta E(r)/2T_c\theta_c$ expression] and noting that $r\approx\bar{u}$ for $r<<1$, it is found that

$$\frac{\Delta E(\bar{u})}{2T_c\theta_c} = \frac{i}{3}\bar{u}^3, \quad \bar{u}<<1 \tag{47}$$

This approximation is valid for all values of i investigated, including $i=1$. It indicates that the mechanism of solid friction damping results from curvature in the force-deflection curve manifested by third-order terms in the power series expansions of the functions at low amplitudes. It is noted that for $i=0$, no energy dissipation exists at low amplitudes, i.e., the force-deflection curve is purely elastic for $\bar{u}<1$. For this reason, the uniform friction model ($i=0$) is viewed as being a degenerate case and of little value in simulating continuous solid friction damping.

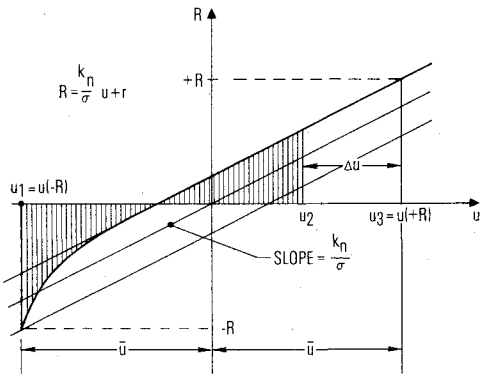

Fig. 7 Energy loss and amplitude decrement per half cycle—nonlinear plus linear spring.

It also is observed that the energy dissipation is proportional to i as indicated in Eq. (47). In addition, it can be shown that the slope of the friction slope functions, given by Eq. (2) and shown in Fig. 2, for $r<<1$ is equal to i. These observations help give some insight to the source of solid friction damping and the characterization of damping by means of the friction model and its parameters.

B. Amplitude Decay Rate

The amplitude decay rate, given by Eq. (38), can be expressed as

$$-\frac{1}{4}\left[\frac{r(\bar{u})}{\bar{u}}+\frac{k_n}{\sigma}\right]\frac{d\bar{u}}{dN} = \frac{1}{\bar{u}}\cdot\frac{\Delta E(\bar{u})}{2T_c\theta_c} \tag{48}$$

The right side of Eq. (48) is the energy dissipation function $\Delta E(\bar{u})/2T_c\theta_c$, divided by $\bar{u}$. Plots of decay rate functions given by Eq. (45) are presented in Fig. 8.

The linear viscous damped oscillator amplitude decay rate given by Eq. (40) can be expressed as

$$\frac{0.25}{2\pi\zeta}\frac{d\bar{u}}{dN} = -0.25\bar{u} \tag{49}$$

in order that the solid friction amplitude decay rates can be compared to that of viscous friction. The factor 0.25 has been

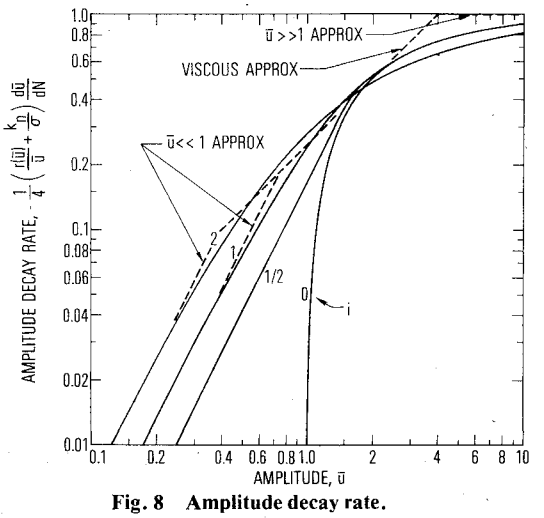

Fig. 8 Amplitude decay rate.

introduced on both sides of Eq. (49) in order to obtain a reasonably good empirical fit of the right side of Eq. (49) with the plotted curves of the right side of Eq. (48).

Figure 8 shows fairly clearly that the curves can be separated into three regions, described as follows

1) Coulomb region

$$\frac{-k_n}{4\sigma}\frac{d\bar{u}}{dN} \approx 1, \quad \bar{u} >> 1 \tag{50}$$

and damping behavior is that of Coulomb friction.

2) Viscous region

$$-\frac{1}{4}\left(\frac{r(\bar{u})}{\bar{u}} + \frac{k_n}{\sigma}\right)\frac{d\bar{u}}{dN} \approx 0.25\bar{u}, \quad \bar{u} \approx 1 \tag{51}$$

where the factor 0.25 is empirical and damping behavior is that of viscous friction.

3) Structural region

$$-\frac{1}{4}\left(1+\frac{k_n}{\sigma}\right)\frac{d\bar{u}}{dN} \approx \frac{i\bar{u}^2}{3}, \quad \bar{u} << 1 \tag{52}$$

and damping behavior is similar to that found in structural damping.

C. Equivalent Linear Damping Ratio

Although the amplitude decay rate functions should describe solid friction damping adequately, it is desirable to describe damping in terms of the equivalent linear damping ratio defined by Eq. (41), which can be expressed in terms of $\bar{u}$

$$\left(\frac{r(\bar{u})}{\bar{u}} + \frac{k_n}{\sigma}\right)\zeta = \frac{2}{\pi\bar{u}^2}\frac{\Delta E(\bar{u})}{2T_c\theta_c} \tag{53}$$

Equation (53) is plotted in Fig. 9. The three regions alluded to are again evident

1) Coulomb region

$$\frac{k_n}{\sigma} - \zeta \approx \frac{2}{\pi\bar{u}}, \quad \bar{u} >> 1 \tag{54}$$

2) Viscous region

$$\left(\frac{r(\bar{u})}{\bar{u}} + \frac{kn}{\sigma}\right)\zeta \approx \frac{1}{2\pi}, \quad \bar{u} \approx 1 \tag{55}$$

3) Structural region

$$\left(1+\frac{k_n}{\sigma}\right)\zeta \approx \frac{2i}{3\pi}\bar{u}, \quad \bar{u} << 1 \tag{56}$$

The first relationship implies that $r/\bar{u}$ is small compared to k_n/σ at large amplitudes, and that the equivalent linear damping ratio is inversely proportional to amplitude. If $k_n = 0$, this approximation obviously is not valid, and the $r/\bar{u}$ term must be used; however, the initial decay in this case will be extremely rapid, and a Coulomb damping phase will not occur. The second relation reveals that solid friction damping appears to be the same as viscous friction when the amplitude is near the value of the characteristic displacement. The last relationship indicates that the equivalent linear damping ratio is proportional to the amplitude of the oscillation $\bar{u}$ at low amplitudes. This is a well-known behaviorial characteristic of structural damping; i.e., the damping ratio or damping factor becomes vanishingly small as the amplitude of oscillation decreases. This characteristic has, in the past, been the basis for assuming or choosing extremely small values of the equivalent linear damping ratio for criteria in the design of high-performance servos and structures. Where an engineering design becomes critically dependent upon knowledge of damping behavior, a nonlinear friction model of the type presented here may be applied fruitfully to represent accurately the physics of structural damping without resorting to restrictively small values of equivalent linear damping ratio.

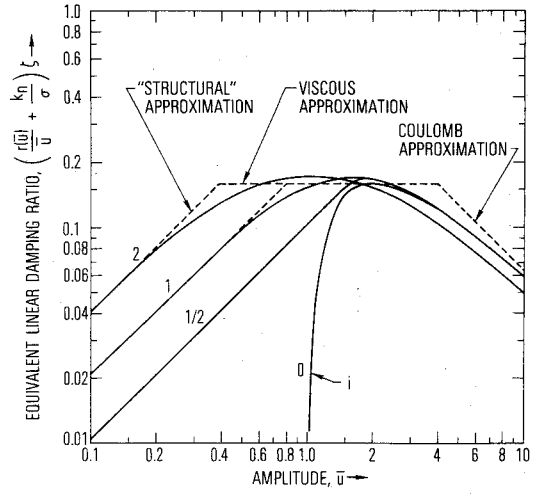

Fig. 9 Equivalent linear damping ratio.

V. Oscillation Decay Envelope

The oscillation decay envelopes for the various solid friction models can be determined using the difference Eq. (31) and the expression for the amplitude decrease per half cycle given by Eq. (36), or by solving the differential Eq. (38). It was found that both approaches give the same result under conditions where the amplitude change per cycle is small. These conditions exist when the linear spring rate is large compared to the nonlinear spring rate, i.e., $k_n/\sigma >> 1$, which was the case for the wire pendulum that was tested. For this reason, the particular case where $k_n/\sigma >> 1$ was considered and amplitude envelopes were obtained. In addition, the case where the linear spring is absent also was investigated.

For the first case, $r(\bar{u})/\bar{u}$ was assumed small compared to k_n/σ everywhere, and Eqs. (36) and (31) were put in the approximation form

$$\Delta u = \frac{\sigma}{k_n}\frac{2[\Delta E(\bar{u})/2T_c\theta_c]}{\bar{u}} \tag{57}$$

$$\bar{u}_{j+1} = \bar{u}_j - \Delta u \tag{58}$$

and the differential Eq. (39) was put in the approximation form

$$\frac{k_n}{\sigma}\frac{d\bar{u}}{dN} = \frac{-2\Delta E(\bar{u})/T_c\theta_c}{\bar{u}} \tag{59}$$

By letting $k_n/\sigma = 4$ in Eq. (57) and using the energy dissipation function for $i = 1$, Eqs. (57) and (58) were solved numerically. The solution is shown in Fig. 10, where $\bar{u}$ is plotted vs $(\sigma/k_n)N$. The initial amplitude $\bar{u} = 10$ was chosen arbitrarily. This solution checks closely with the solution obtained for the differential Eq. (59). However, if k_n/σ is set equal to 1.0, the difference equation solution deviates from the differential equation solution excessively at the larger amplitudes (i.e., $\bar{u} \gtrsim 1$) due to approximations made in Eq. (28). The differential equation therefore is regarded as providing a better description of the continuous decay envelope, although the difference equation realistically describes the decay as a discrete process.

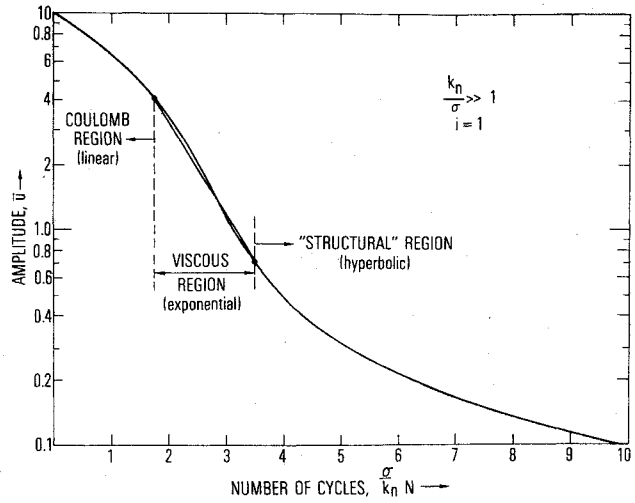

Fig. 10 Oscillator decay envelope.

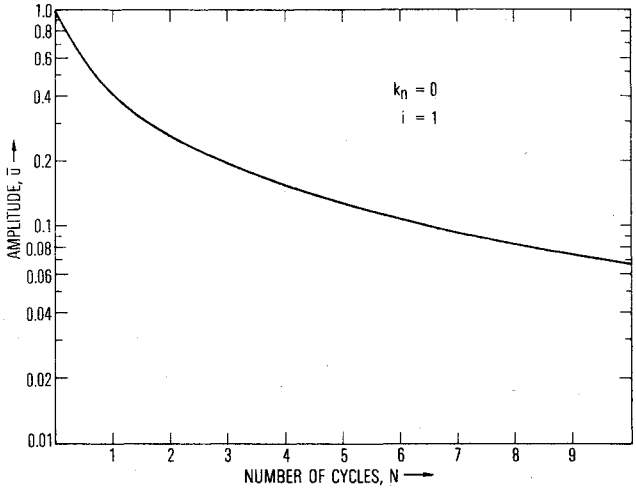

Fig. 11 "Structural" decay envelope.

Figure 10 shows the three regions described previously. If solutions to Eqs. (50-52) are obtained with the initial condition $u=u_0$ at $N=0$ under the assumption that $k_n/\sigma >> 1$, the three amplitude decay regions in Fig. 10 can be described as follows

a) Coulomb region

$$(\bar{u}-\bar{u}_0) = -4(\sigma/k_n)N, \quad \bar{u} \gtrsim 4 \tag{60}$$

and the envelope decay is linear with N.

b) Viscous region

$$\bar{u} = \bar{u}_0 \exp\left[-\left(\frac{\sigma}{k_n}N\right)\right], \quad 4 \gtrsim \bar{u} \gtrsim 0.7 \tag{61}$$

and the envelope decay is exponential with N.

c) Structural region

$$\bar{u} = \left(\frac{4i}{3}\frac{\sigma}{k_n}N + \frac{1}{\bar{u}_0}\right)^{-1}, \quad \bar{u} \lesssim 0.7 \tag{62}$$

and the envelope decay is hyperbolic with N.

In the Coulomb region, the decay envelope is described by Eq. (60), which corresponds to the linear decay envelope of classical Coulomb friction given by Eq. (20).

In the viscous region in the semilog plot of Fig. 10, the exponential decay envelope is approximately a straight line from $\bar{u} \approx 4$ to $\bar{u} \approx 0.7$. The constant slope line on the figure in this range has a slope that corresponds to the linear equivalent damping ratio empirical value of $0.16 \approx 1/2\pi$. This is indicated in Fig. 9 as the constant value of the approximate equivalent linear damping ratio in the same region.

In the structural region, the amplitude $\bar{u}$ varies inversely with N and, hence, the decay envelope is described as hyperbolic and approaches zero asymptotically. The time required to reduce amplitude by a given percentage can be shown from Eq. (62) to be proportional to amplitude. This is a way of saying that the equivalent linear damping ratio is proportional to the amplitude. This is not to say, however, that the solid friction damping mechanism ceases at low levels. In fact, it seems important to draw the conclusion that the classical concept of viscous damping should be set aside at low amplitudes, and the decay envelope should be viewed simply as being hyperbolic rather than exponential.

For the second case where the linear spring is absent, $k_n = 0$ and the differential Eq. (38) can be put in the approximation form

$$\frac{d\bar{u}}{dN} \approx \frac{2\Delta E(\bar{u})/T_c\theta_c}{r(\bar{u})} \tag{63}$$

A computer solution of Eq. (63) was obtained and is shown in Fig. 11. The plot of $\bar{u}$ vs N starts at $\bar{u}=1$ rather than $\bar{u}=10$ as in Fig. 10, because the extremely high decay rate values for $\bar{u}>1$ indicate that the motion will be damped to $\bar{u}<1$ in the first half cycle or so. It is observed, however, that the decay envelope in Fig. 11 is almost identical to that of Fig. 10 for $\bar{u} \lesssim 0.7$, which is the "structural region." The case where $k_n = 0$ therefore is seen to apply to structural materials; hence, the name given this region is appropriate.

The general case where both terms $r/\bar{u}$ and k_n/σ are considered is not treated here. However, the character of the decay envelopes for the general case will be similar to those analyzed.

VI. Conclusions

The solid friction models behave like Coulomb friction at large amplitudes of oscillation, and the amplitude decay envelopes decrease linearly with the number of cycles or with time. The behavior is similar to viscous friction when the amplitude of oscillation is near the characteristic displacement x_c and the amplitude decay envelopes decrease exponentially with the number of cycles.

At low amplitudes, the solid friction models behave in a way that is described as "structural" damping, wherein the equivalent linear damping ratio varies directly with the amplitude of oscillation. In the low-amplitude range, the amplitude decay envelopes decrease hyperbolically with the number of cycles or with time.

The "structural" equivalent damping ratio is proportional to the exponent i in the solid friction model which characterizes the curvature on the load-deflection curve of the solid friction material.

Computer simulations using the solid friction models will, of course, obviate the need for extensive analysis in most problems where the solid friction models are applied. Simulation is certainly the approach to take in the study of large, high-order state equation systems. The usefulness of the second-order nonlinear oscillator analysis presented here lies in gaining insight and understanding of friction damping behavior.

References

[1] Dahl, P.R., "A Solid Friction Model," TOR-158(3107-18), May 1968, The Aerospace Corporation, El Segundo, Calif.

[2] Kuo, B.C., Singh, G., and Seltzer, S.M., "Stability Study of the Large Space Telescope (LST) System with Nonlinear CMG Gimbal Friction," AIAA Paper 74-874, Anaheim, Calif., 1974.

[3] Nurre, G.S., "An Analysis of the Dahl Friction Model and Its Effect on a CMG Gimbal Rate Controller," NASA-TMX 64934, Oct. 1974.

[4]Jacot, A.D. and Emsley, W.W., "Assessment of Fine Stabilization Problems for the LST," AIAA Paper 73-881, Key Biscayne, Fla., 1973.

[5]Osborne, N.A. and Rittenhouse, D.L., "The Modeling of Friction and Its Effects on Fine Pointing Control," AIAA Paper 74-875, Anaheim, Calif., 1974.

[6]Seltzer, S.M., "Large Space Telescope Oscillations Included by CMG Friction," *Journal of Spacecraft and Rockets,* Vol. 12, Feb. 1975, pp. 96-105.

[7]Iwan, W.D., "A Distributed-Element Model for Hysteresis and Its Steady State Dynamic Response," *Journal of Applied Mechanics, Transactions of the ASME,* Vol. 33, Dec. 1966, pp. 893-900.

[8]Ramberg, W. and Osgood, W.R., "Description of Stress-Strain Curves by Three Parameters," NACA TN 902, 1943.

This article has been cited by:

1. Malte Krack, Lars Panning-von Scheidt, Jörg Wallaschek. 2013. On the computation of the slow dynamics of nonlinear modes of mechanical systems. *Mechanical Systems and Signal Processing* . [CrossRef]
2. Sung Jig Kim. 2013. Seismic Performance Assessment of a Nonlinear Structure Controlled by Magneto-Rheological Damper Using Multi-Platform Analysis. *Journal of the Earthquake Engineering Society of Korea* **17**:3, 143-150. [CrossRef]
3. Ruiyue Ouyang, Vincent Andrieu, Bayu Jayawardhana. 2013. On the characterization of the Duhem hysteresis operator with clockwise input–output dynamics. *Systems & Control Letters* **62**:3, 286-293. [CrossRef]
4. Paweł Gutowski, Mariusz Leus. 2012. The effect of longitudinal tangential vibrations on friction and driving forces in sliding motion. *Tribology International* **55**, 108-118. [CrossRef]
5. Jianxun Liang, Steven Fillmore, Ou Ma. 2012. An extended bristle friction force model with experimental validation. *Mechanism and Machine Theory* **56**, 123-137. [CrossRef]
6. Ming Xu, Xiao-Ling Jin, Zhi-Long Huang. 2012. First-passage failure of Duhem hysteretic systems. *Acta Mechanica* **223**:9, 1959-1970. [CrossRef]
7. Elena Syerko, Sébastien Comas-Cardona, Christophe Binetruy. 2012. Models of mechanical properties/behavior of dry fibrous materials at various scales in bending and tension: A review. *Composites Part A: Applied Science and Manufacturing* **43**:8, 1365-1388. [CrossRef]
8. Jia He, Bin Xu, Sami F. Masri. 2012. Restoring force and dynamic loadings identification for a nonlinear chain-like structure with partially unknown excitations. *Nonlinear Dynamics* **69**:1-2, 231-245. [CrossRef]
9. Fatemeh Pourahmadian, Hamid Ahmadian, Hassan Jalali. 2012. Modeling and identification of frictional forces at a contact interface experiencing micro-vibro-impacts. *Journal of Sound and Vibration* **331**:12, 2874-2886. [CrossRef]
10. N. Aguirre, F. Ikhouane, J. Rodellar, R. Christenson. 2012. Parametric identification of the Dahl model for large scale MR dampers. *Structural Control and Health Monitoring* **19**:3, 332-347. [CrossRef]
11. Quentin Bombled, Olivier Verlinden. 2012. Dynamic simulation of six-legged robots with a focus on joint friction. *Multibody System Dynamics* . [CrossRef]
12. Bin Xu, Jia He, Sami F. Masri. 2012. Data-based Identification of nonlinear restoring force under spatially incomplete excitations with power series polynomial model. *Nonlinear Dynamics* **67**:3, 2063-2080. [CrossRef]
13. Yo KOBAYASHI, Takahiro SATO, Takeharu HOSHI, Masakatsu G. FUJIE. 2012. Frictional Force Modeling Ranging from Hyper to Slow Relative Velocity between a Needle and Liver Tissue. *Journal of Biomechanical Science and Engineering* **7**:3, 305-317. [CrossRef]
14. Wolf R. Krüger, Marco Morandini. 2011. Recent developments at the numerical simulation of landing gear dynamics. *CEAS Aeronautical Journal* **1**:1-4, 55-68. [CrossRef]
15. Z Jiang, R Christenson. 2011. A comparison of 200 kN magneto-rheological damper models for use in real-time hybrid simulation pretesting. *Smart Materials and Structures* **20**:6, 065011. [CrossRef]
16. Jesús Sandoval, Rafael Kelly, Víctor Santibáñez. 2011. Interconnection and damping assignment passivity-based control of a class of underactuated mechanical systems with dynamic friction. *International Journal of Robust and Nonlinear Control* **21**:7, 738-751. [CrossRef]
17. Hassan Jalali, Hamid Ahmadian, Fatemeh Pourahmadian. 2011. Identification of micro-vibro-impacts at boundary condition of a nonlinear beam. *Mechanical Systems and Signal Processing* **25**:3, 1073-1085. [CrossRef]
18. Jan Høgsberg. 2011. The role of negative stiffness in semi-active control of magneto-rheological dampers. *Structural Control and Health Monitoring* **18**:3, 289-304. [CrossRef]
19. D H Wang, W H Liao. 2011. Magnetorheological fluid dampers: a review of parametric modelling. *Smart Materials and Structures* **20**:2, 023001. [CrossRef]
20. Syh-Shiuh Yeh, Hsin-Chun Su. 2011. Development of friction identification methods for feed drives of CNC machine tools. *The International Journal of Advanced Manufacturing Technology* **52**:1-4, 263-278. [CrossRef]
21. A. Bazaei, M. Moallem. 2011. Friction Hysteresis Modeling and Force Control in a Constrained Single-link Arm. *Journal of Dynamic Systems, Measurement, and Control* **133**:6, 061016. [CrossRef]
22. Michael A. Guthrie, Daniel C. Kammer. 2011. A Reduction Procedure for One-Dimensional Joint Models and Application to a Lap Joint. *Journal of Vibration and Acoustics* **133**:3, 031002. [CrossRef]
23. Alfred Zmitrowicz. 2010. Contact stresses: a short survey of models and methods of computations. *Archive of Applied Mechanics* **80**:12, 1407-1428. [CrossRef]

24. Jian-jun Qu, Ning-ning Zhou, Yan-li Wang. 2010. Experimental study of air squeeze effect on high-frequency friction contact. *Tribology International* **43**:11, 2190-2195. [CrossRef]
25. Hamid Ahmadian, Hassan Jalali, Fatemeh Pourahmadian. 2010. Nonlinear model identification of a frictional contact support. *Mechanical Systems and Signal Processing* **24**:8, 2844-2854. [CrossRef]
26. E. Bilbao, D. Soulat, G. Hivet, A. Gasser. 2010. Experimental Study of Bending Behaviour of Reinforcements. *Experimental Mechanics* **50**:3, 333-351. [CrossRef]
27. İ Şahin, T Engin, Ş Çeşmeci. 2010. Comparison of some existing parametric models for magnetorheological fluid dampers. *Smart Materials and Structures* **19**:3, 035012. [CrossRef]
28. Olivier A. Bauchau, Yannick Van Weddingen, Sandeep Agarwal. 2010. Semiactive Coulomb Friction Lead-Lag Dampers. *Journal of the American Helicopter Society* **55**:1, 012005. [CrossRef]
29. A. Bazaei, M. Moallem. 2010. Presticition Friction Modeling and Position Control in an Actuated Rotary Arm. *IEEE Transactions on Instrumentation and Measurement* **59**:1, 131-139. [CrossRef]
30. A. Caignot, P. Ladevèze, D. Néron, J.-F. Durand. 2010. Virtual testing for the prediction of damping in joints. *Engineering Computations* **27**:5, 621-644. [CrossRef]
31. Jean-Luc Dion, Sylvie Le Moyne, Gaël Chevallier, Hamidou Sebbah. 2009. Gear impacts and idle gear noise: Experimental study and non-linear dynamic model. *Mechanical Systems and Signal Processing* **23**:8, 2608-2628. [CrossRef]
32. M. H. Korayem, S. Sadeghzadeh. 2009. A new modeling and compensation approach for creep and hysteretic loops in nanosteering by SPM's piezotubes. *The International Journal of Advanced Manufacturing Technology* **44**:11-12, 1133-1143. [CrossRef]
33. Carlo Cantoni, Riccardo Cesarini, Giampiero Mastinu, Gianpiero Rocca, Roberto Sicigliano. 2009. Brake comfort – a review. *Vehicle System Dynamics* **47**:8, 901-947. [CrossRef]
34. Denis Laxalde, Fabrice Thouverez. 2009. Complex non-linear modal analysis for mechanical systems: Application to turbomachinery bladings with friction interfaces. *Journal of Sound and Vibration* **322**:4-5, 1009-1025. [CrossRef]
35. V. Hayward, B.S.R. Armstrong, F. Altpeter, P.E. Dupont. 2009. Discrete-Time Elasto-Plastic Friction Estimation. *IEEE Transactions on Control Systems Technology* **17**:3, 688-696. [CrossRef]
36. G. Aridon, D. Rémond, F. Morestin, L. Blanchard, R. Dufour. 2009. Self-Deployment of a Tape-Spring Hexapod: Experimental and Numerical Investigation. *Journal of Mechanical Design* **131**:2, 021003. [CrossRef]
37. Wen-Fang Xie, Jun Fu, Han Yao, C.-Y. Su. 2009. Neural network-based adaptive control of piezoelectric actuators with unknown hysteresis. *International Journal of Adaptive Control and Signal Processing* **23**:1, 30-54. [CrossRef]
38. Fakhreddine Landolsi, Fathi H. Ghorbel, Jun Lou, Hao Lu, Yuekai Sun. 2009. Nanoscale Friction Dynamic Modeling. *Journal of Dynamic Systems, Measurement, and Control* **131**:6, 061102. [CrossRef]
39. Xiong-liang Yao, Zheng-dong Tian, Zhi-hua Shen, Shao-jing Guo. 2008. Research on low-frequency mechanical characteristics of the MR dampers in ship isolators. *Journal of Marine Science and Application* **7**:4, 243-247. [CrossRef]
40. Stefania Gualdi, Marco Morandini, Gian Luca Ghiringhelli. 2008. Anti-skid induced aircraft landing gear instability. *Aerospace Science and Technology* **12**:8, 627-637. [CrossRef]
41. Bibliography 549-602. [CrossRef]
42. Jan Høgsberg, Steen Krenk. 2008. Energy dissipation control of magneto-rheological damper. *Probabilistic Engineering Mechanics* **23**:2-3, 188-197. [CrossRef]
43. X. W Tangpong, J. A Wickert, A. Akay. 2008. Distributed friction damping of travelling wave vibration in rods. *Philosophical Transactions of the Royal Society A: Mathematical, Physical and Engineering Sciences* **366**:1866, 811-827. [CrossRef]
44. Chen Hsieh, Gi-Lung Lin. 2008. Modeling and Micro-Radian Precision Pointing of a Flexible Manipulator With the Existence of Static Friction. *IEEE Transactions on Control Systems Technology* **16**:1, 148-157. [CrossRef]
45. Xiaobin Lu, M. M. Khonsari. 2008. An Experimental Study of Oil-Lubricated Journal Bearings Undergoing Oscillatory Motion. *Journal of Tribology* **130**:2, 021702. [CrossRef]
46. Chen. 2008. Haptic Rendering of Three-dimensional Heterogeneous Fine Surface Features. *Computer-Aided Design and Applications* **5**. . [CrossRef]
47. Mohsen Mahvash, Allison Okamura. 2007. Friction Compensation for Enhancing Transparency of a Teleoperator With Compliant Transmission. *IEEE Transactions on Robotics* **23**:6, 1240-1246. [CrossRef]
48. E. Pennestrì, P. P. Valentini, L. Vita. 2007. Multibody dynamics simulation of planar linkages with Dahl friction. *Multibody System Dynamics* **17**:4, 321-347. [CrossRef]

49. Carlos Canudas-de-Wit, Rafael Kelly. 2007. PASSIVITY ANALYSIS OF A MOTION CONTROL FOR ROBOT MANIPULATORS WITH DYNAMIC FRICTION. *Asian Journal of Control* **9**:1, 30-36. [CrossRef]
50. Nguyen B. Do, Aldo A. Ferri, Olivier A. Bauchau. 2007. Efficient Simulation of a Dynamic System with LuGre Friction. *Journal of Computational and Nonlinear Dynamics* **2**:4, 281. [CrossRef]
51. P. Herman. 2007. Velocity controller with friction compensation. *IET Control Theory & Applications* **1**:1, 238. [CrossRef]
52. Hard Disk Drive Mechatronics and Control **20066043**, 335-353. [CrossRef]
53. M.H. Perng, S.H. Wu. 2006. A fast control law for nano-positioning. *International Journal of Machine Tools and Manufacture* **46**:14, 1753-1763. [CrossRef]
54. Olivier A. Bauchau, Changkuan Ju. 2006. Modeling friction phenomena in flexible multibody dynamics. *Computer Methods in Applied Mechanics and Engineering* **195**:50-51, 6909-6924. [CrossRef]
55. Q. Zhou, S.R.K. Nielsen, W.L. Qu. 2006. Semi-active control of three-dimensional vibrations of an inclined sag cable with magnetorheological dampers. *Journal of Sound and Vibration* **296**:1-2, 1-22. [CrossRef]
56. Chein-Shan Liu, Po-Jui Su. 2006. Steady-state responses of a compliant friction slider under harmonic excitations. *Journal of the Chinese Institute of Engineers* **29**:3, 549-555. [CrossRef]
57. Joško Deur, Jahan Asgari, Davor Hrovat. 2006. Modeling and Analysis of Automatic Transmission Engagement Dynamics-Nonlinear Case Including Validation. *Journal of Dynamic Systems, Measurement, and Control* **128**:2, 251. [CrossRef]
58. Javier Moreno-Valenzuela, Rafael Kelly. 2006. A Hierarchical Approach to Manipulator Velocity Field Control Considering Dynamic Friction Compensation. *Journal of Dynamic Systems, Measurement, and Control* **128**:3, 670. [CrossRef]
59. JAN AWREJCEWICZ, PAWEŁ OLEJNIK. 2005. FRICTION PAIR MODELING BY A 2-DOF SYSTEM: NUMERICAL AND EXPERIMENTAL INVESTIGATIONS. *International Journal of Bifurcation and Chaos* **15**:06, 1931-1944. [CrossRef]
60. Ryuta SATO, Masaomi TSUTSUMI. 2005. Mathematical Model of Feed Drive Systems Consisting of AC Servo Motor and Linear Ball Guide. *Journal of the Japan Society for Precision Engineering, Contributed Papers* **71**:5, 633-638. [CrossRef]
61. J. Awrejcewicz, P. Olejnik. 2005. Analysis of Dynamic Systems With Various Friction Laws. *Applied Mechanics Reviews* **58**:6, 389. [CrossRef]
62. Carlos Canudas-de-Wit, Hubert Bechart, Xavier Claeys, Pietro Dolcini, John-Jairo Martinez. 2005. Fun-to-Drive by Feedback*. *European Journal of Control* **11**:4-5, 353-383. [CrossRef]
63. A.M. Okamura, C. Simone, M.D. O'Leary. 2004. Force Modeling for Needle Insertion Into Soft Tissue. *IEEE Transactions on Biomedical Engineering* **51**:10, 1707-1716. [CrossRef]
64. C.L. Chen, M.J. Jang, K.C. Lin. 2004. Modeling and high-precision control of a ball-screw-driven stage. *Precision Engineering* **28**:4, 483-495. [CrossRef]
65. Taejung Kim, Seung-kil Son, Sanjay E. Sarma. 2004. On actuator reversal motions of machine tools. *Mechanism and Machine Theory* **39**:3, 299-322. [CrossRef]
66. E. P. Petrov, D. J. Ewins. 2004. Generic Friction Models for Time-Domain Vibration Analysis of Bladed Disks. *Journal of Turbomachinery* **126**:1, 184. [CrossRef]
67. Ying Zuguang. 2003. Response analysis of randomly excited nonlinear systems with symmetric weighting Preisach hysteresis. *Acta Mechanica Sinica* **19**:4, 365-370. [CrossRef]
68. Ting-Yung Lin, Yih-Chieh Pan, Chen Hsieh. 2003. Precision-limit positioning of direct drive systems with the existence of friction. *Control Engineering Practice* **11**:3, 233-244. [CrossRef]
69. J. Moreno, R. Kelly, R. Campa. 2003. Manipulator velocity control using friction compensation. *IEE Proceedings - Control Theory and Applications* **150**:2, 119. [CrossRef]
70. Y.Q. Ni, Z.G. Ying, J.M. Ko, W.Q. Zhu. 2002. Random response of integrable Duhem hysteretic systems under non-white excitation. *International Journal of Non-Linear Mechanics* **37**:8, 1407-1419. [CrossRef]
71. Jian Qin Gong, Lin Guo, Ho Seong Lee, Bin Yao. 2002. Modeling and cancellation of pivot nonlinearity in hard disk drives. *IEEE Transactions on Magnetics* **38**:5, 3560-3565. [CrossRef]
72. D. Abramovitch, G. Franklin. 2002. A brief history of disk drive control. *IEEE Control Systems* **22**:3, 28-42. [CrossRef]
73. P. Dupont, V. Hayward, B. Armstrong, F. Altpeter. 2002. Single state elastoplastic friction models. *IEEE Transactions on Automatic Control* **47**:5, 787-792. [CrossRef]
74. Adnan Akay. 2002. Acoustics of friction. *The Journal of the Acoustical Society of America* **111**:4, 1525. [CrossRef]

75. Olivier A. Bauchau, Jesus Rodriguez, Carlo L. Bottasso. 2001. Modeling of unilateral contact conditions with application to aerospace systems involving backlash, freeplay and friction. *Mechanics Research Communications* **28**:5, 571-599. [CrossRef]
76. Jun Ni, Zhenqi Zhu. 2001. Experimental Study of Tangential Micro Deflection of Interface of Machined Surfaces. *Journal of Manufacturing Science and Engineering* **123**:2, 365. [CrossRef]
77. Chen Hsieh, Y.-C. Pan. 2000. Dynamic behavior and modelling of the pre-sliding static friction. *Wear* **242**:1-2, 1-17. [CrossRef]
78. Harry Dankowicz, Arne B. Nordmark. 2000. On the origin and bifurcations of stick-slip oscillations. *Physica D: Nonlinear Phenomena* **136**:3-4, 280-302. [CrossRef]
79. Jun Oh Jang, Gi Joon Jeon. 2000. A parallel neuro-controller for DC motors containing nonlinear friction. *Neurocomputing* **30**:1-4, 233-248. [CrossRef]
80. Steven J. Bullock, Lee D. Peterson. 1999. Nanometer Regularity in the Mechanics of a Precision Deployable Spacecraft Structure Joint. *Journal of Spacecraft and Rockets* **36**:5, 758-764. [Citation] [PDF] [PDF Plus]
81. Ulf Sellgren, Ulf Olofsson. 1999. Application of a constitutive model for micro-slip in finite element analysis. *Computer Methods in Applied Mechanics and Engineering* **170**:1-2, 65-77. [CrossRef]
82. Seon-Woo Lee, Jong-Hwan Kim. 1999. Friction Identification Using Evolution Strategies and Robust Control of Positioning Tables. *Journal of Dynamic Systems, Measurement, and Control* **121**:4, 619. [CrossRef]
83. Paul C. Mitiguy, Arun K. Banerjee. 1999. Efficient Simulation of Motions Involving Coulomb Friction. *Journal of Guidance, Control, and Dynamics* **22**:1, 78-86. [Citation] [PDF] [PDF Plus]
84. B. Li, D. Hullender, M. DiRenzo. 1998. Nonlinear induced disturbance rejection in inertial stabilization systems. *IEEE Transactions on Control Systems Technology* **6**:3, 421-427. [CrossRef]
85. Lars A Hagman, Ulf Olofsson. 1998. A model for micro-slip between flat surfaces based on deformation of ellipsoidal elastic asperities—parametric study and experimental investigation. *Tribology International* **31**:4, 209-217. [CrossRef]
86. Wodek Gawronski, Ben Parvin. 1998. Radiotelescope Low-Rate Tracking Using Dither. *Journal of Guidance, Control, and Dynamics* **21**:2, 349-352. [Citation] [PDF] [PDF Plus]
87. H. D. Taghirad, P. R. Bélanger. 1998. Modeling and Parameter Identification of Harmonic Drive Systems. *Journal of Dynamic Systems, Measurement, and Control* **120**:4, 439. [CrossRef]
88. H. Olsson, K.J. Åström, C. Canudas de Wit, M. Gäfvert, P. Lischinsky. 1998. Friction Models and Friction Compensation. *European Journal of Control* **4**:3, 176-195. [CrossRef]
89. Wodek Gawronski, Ben Parvin, Wodek Gawronski, Ben ParvinRadiotelescope low rate tracking using dither . [Citation] [PDF] [PDF Plus]
90. Ulf Olofsson, Lars Hagman. 1997. A model for micro-slip between flat surfaces based on deformation of ellipsoidal elastic bodies. *Tribology International* **30**:8, 599-603. [CrossRef]
91. K. Eddy, J. Steele, W. Messner. 1997. Bias in disk drive rotary actuators: characterization, prediction, and compensation. *IEEE Transactions on Magnetics* **33**:3, 2424-2436. [CrossRef]
92. Arun K. Banerjee, Thomas R. Kane. 1994. Modeling and simulation of rotor bearing friction. *Journal of Guidance, Control, and Dynamics* **17**:5, 1137-1139. [Citation] [PDF] [PDF Plus]
93. A. P. Mazzoleni, A. L. Schlack. 1994. Comparative stability study illustrating advantages of guy-wire constraints for flexible satellites. *Journal of Guidance, Control, and Dynamics* **17**:5, 1139-1141. [Citation] [PDF] [PDF Plus]
94. Brian Armstrong-Hélouvry, Pierre Dupont, Carlos Canudas De Wit. 1994. A survey of models, analysis tools and compensation methods for the control of machines with friction. *Automatica* **30**:7, 1083-1138. [CrossRef]
95. S. Cetinkunt, W.L. Yu, J. Filliben, A. Donmez. 1994. Friction characterization experiments on a single point diamond turning machine tool. *International Journal of Machine Tools and Manufacture* **34**:1, 19-32. [CrossRef]
96. K. O. PRAKAH-ASANTE, A. S. ISLAM, D. WALCZYK, K. CRAIG. 1993. Design, Construction and Testing of a Single-axis Servomechanism for Control Experiments involving Coulomb Friction, Backlash and Joint Compliance. *Journal of Engineering Design* **4**:4, 305-329. [CrossRef]